SIGNAL CONSTELLATION DISTORTION AND BER DEGRADATION DUE TO HARDWARE IMPAIRMENTS IN SIX-PORT RECEIVERS WITH ANALOG I/Q GENERATION

A. Moscoso-Martir[*], I. Molina-Fernandez, and A. Ortega-Moñux

Departmento de Ingenieria de Comunicaciones, ETSI Telecomunicacion, Malaga University, Campus Universitario de Teatinos s/n, Malaga 29011, Spain

Abstract—Since its introduction in 1994 direct conversion six-port receivers have attracted a considerable attention at microwave frequencies, with most recent work focusing on the so called six-port receivers with analog I/Q generation. Besides its applications at microwave frequencies, six-port receivers with I/Q regeneration play a crucial role in the optical communications field, as they are the most promising candidates for optical coherent receivers that are being developed for 100 Gigabit Ethernet transceivers. In this paper we analytically model the influence of six-port junction hardware impairments on receiver performance. New analytical expressions are developed which give geometrical interpretation of signal constellation distortion due to hardware impairments and allow for the definition of several interesting figures of merit. Closed formulas are also proposed to analytically calculate BER degradation, under AWGN conditions, from these figures of merit. Finally, the proposed formulas are validated by means of simulation, and it is shown that they can be of practical interest to set the specifications of the six-port junction components.

1. INTRODUCTION

Modern wireless microwave receiver design demands increased bandwidth with reduced size and cost. Since its introduction in 1994 [1] direct conversion six-port receivers have attracted a considerable

attention at microwave frequencies [2–4] as they offer lower hardware complexity, lower local oscilator (LO) power, and higher bandwidth when compared with other alternatives that make use of active mixers. Besides, six-port based direct detection receivers are nowadays a hot topic in the optical community as they are the most promising candidates for modern 100 Gb/s coherent optical receivers [5–7].

Figure 1 shows the basic building blocks of a six-port receiver: the six-port passive junction and the four power detectors. The six-port passive junction combines the reference signal, generated by the local oscillator (LO), and the received radio frequency (RX) signal, with specific amplitude and phase relations at the input of the four power detectors. Six-port receivers are usually designed to work in homodyne operation, so that, the power detector outputs are directly obtained in baseband, and the I/Q signals can be recovered by analog or digital means. In the first six-port receiver proposals [1] the four power detectors outputs were digitized, which enabled the use of powerful calibration strategies to remove hardware imperfections [8]. However, more recently, analog I/Q generation has become the preferred alternative. It offers the advantage of providing a simple analog solution at the cost of requiring a much more demanding hardware design (as no calibration is available).

Several papers have studied the performance and features of six-port receiver with analog I/Q generation in multiple situations. In [9] the six-port receiver is theoretically described and compared with the homodyne and heterodyne reception architectures. In [10] the analysis is focused on the relationship between the LO power level and system level parameters of the receiver with an ideal six-port network. Finally, in [11] the diode power detector behavior in a six-port communications receiver is studied using an ideal six-port network. However, up to the authors' knowledge, a complete study of the influence of six-port junction hardware impairments on receiver performance has not been reported yet.

The goal of this paper is to make a detailed study of the performance degradation of analog I/Q generation six-port receivers due to hardware imperfections of the six-port passive junction. Ideal square law power detector behaviour is considered throughout this work. Compact expressions are obtained that give a deeper insight into the mechanisms causing receiver degradation due to hardware impairments. Furthermore, they allow to easily calculate the Error Vector Magnitude (EVM) and to set hardware specifications to fulfill the design requirements. Specific theoretical formulas are also presented to calculate Bit Error Rate (BER) degradation for a QPSK modulation scheme. Finally, assessment of the proposed formulas is

carried out by comparison with numerical simulations of a six-port, showing an excellent agreement.

This paper is organized as follows. Section 2 analysis the six-port receiver with analog I/Q generation. Section 3 studies the symbol constellation distortion due to six-port hardware impairments using the equations obtained in Section 2. Section 4 quantifies the effects of hardware impairments in these type of receivers by developing a closed expression to calculate the Error Vector Magnitude (EVM). Section 5 determines the error probability of six-port receiver from EVM when a QPSK modulation is used. Section 6 analyses a specific six-port architecture to get a deeper insight into its behavior. Section 7 validates the main formulas proposed in this paper by simulations. Finally, Section 8 presents the conclusions of this paper.

2. THEORY OF SIX-PORT RECEIVER WITH ANALOG I/Q GENERATION

2.1. Ideal I/Q Demodulator

Before presenting the particular behavior of the six-port receiver, it is convenient to analyze which is the ideal functionality required for an ideal I/Q demodulator. Referring to Fig. 1, considering a homodyne situation (with equal RX and LO frequencies $\omega_{\mathrm{RX}} = \omega_{\mathrm{LO}}$) and using complex envelope formalism, we can write

$$\begin{aligned} e_{\mathrm{RX}}(t) &= Re\left\{\widetilde{e}_{\mathrm{RX}}\exp\left(j\omega_0 t\right)\right\} \\ e_{\mathrm{LO}}(t) &= Re\left\{\widetilde{e}_{\mathrm{LO}}\exp\left(j\omega_0 t\right)\right\} \end{aligned}, \tag{1}$$

where $\widetilde{e}_{\mathrm{RX}}$ and $\widetilde{e}_{\mathrm{LO}}$ are complex numbers. Then, the received symbol Γ^{RX} can be defined in the complex plane as the (complex) ratio

$$\Gamma^{\mathrm{RX}} = \frac{\widetilde{e}_{\mathrm{RX}}}{\widetilde{e}_{\mathrm{LO}}} = I^{\mathrm{RX}} + jQ^{\mathrm{RX}}, \tag{2}$$
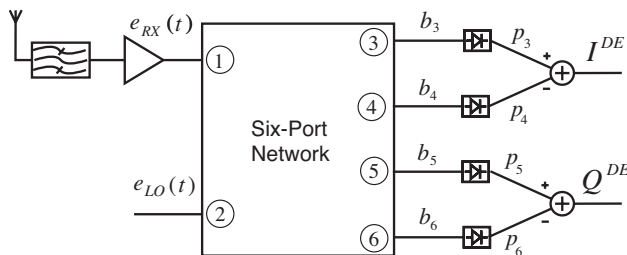

Figure 1. Basic block diagram of a general six-port receiver with analog I/Q generation.
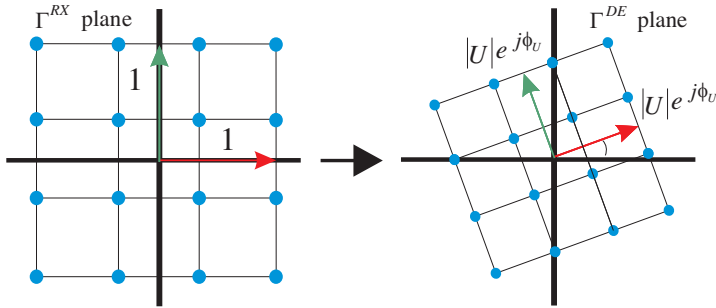
Figure 2. Transformation between the received (Γ^{RX}) and demodulated (Γ^{DE}) symbol planes caused by the demodulator in an ideal situation.

whose amplitude is the ratio of the RX to LO amplitude and its phase is the phase difference between RX and LO signals. The I/Q demodulator aims to recover a demodulated symbol

$$\Gamma^{\mathrm{DE}} = I^{\mathrm{DE}} + jQ^{\mathrm{DE}} \tag{3}$$

so that, in the ideal situation, Γ^{DE} equals Γ^{RX} except for an arbitrary complex constant for all the possible constellation symbols, i.e.,

$$\Gamma^{\mathrm{ID}} = \Gamma^{\mathrm{DE}} = U\,\Gamma^{\mathrm{RX}} \tag{4}$$

where the ID super-index indicates ideal demodulation. It must be noticed that, from a communications receiver point of view, the arbitrary constant value, U, is irrelevant, as its amplitude $|U|$ and phase ϕ_U will be subsequently adjusted by receiver Automatic Gain Control (AGC) and Carrier Recovery Subsystem, respectively. This situation is illustrated in Fig. 2 where it is graphically shown that in an ideal case, a demodulator establishes a transformation between the received (Γ^{RX}) and demodulated (Γ^{DE}) symbol planes which should ideally consist of a simple scaling and rotation that can be easily corrected.

2.2. Six-port Demodulator Equations

Figure 1 shows a general six-port receiver with analog I/Q generation. It is comprised of a passive six-port junction with two input ports, RX ($e_{\mathrm{RX}}(t)$) and LO ($e_{\mathrm{LO}}(t)$), and four outputs with suitable power detectors. For perfectly matched square law detectors, output power waves are linear combinations of the RX and LO waves, i.e.,

$$p_i = R_i \left| \widetilde{b}_i \right|^2 = R_i \left| S_{i1}\widetilde{e}_{\mathrm{RX}} + S_{i2}\widetilde{e}_{\mathrm{LO}} \right|^2 \ i = 3, \ldots, 6, \tag{5}$$

where S_{ik} are six-port junction scattering parameters and R_i are the power detector sesitivities. This result can be easily generalized to include non ideally matched detectors. Defining: i) LO power as $P_{LO} = |\tilde{e}_{LO}|^2$, ii) port sensitivity as $k_i = R_i |S_{i1}|^2$ and six-port centres as $q_i = -\frac{S_{i2}}{S_{i1}}$, which play a central role in six-port theory [12], (5) can be rewritten as:

$$p_i = P_{LO} k_i \left[|q_i|^2 + |\Gamma^{RX}|^2 - 2Re\left(q_i^* \Gamma^{RX}\right) \right] = i = 3, \ldots, 6. \quad (6)$$

As seen in Fig. 1, in analog I/Q regeneration receivers two pair of outputs are analogically subtracted to obtain the in-phase (I^{DE}) and quadrature (Q^{DE}) channels of the recovered signal. These output channels can be normalized by P_{LO} yielding

$$\overline{I^{DE}} = \frac{p_3 - p_4}{P_{LO}} = \alpha_I + \gamma_i \left|\Gamma^{RX}\right|^2 + Re\left(u^* \Gamma^{RX}\right), \quad (7)$$

$$\overline{Q^{DE}} = \frac{p_5 - p_6}{P_{LO}} = \alpha_Q + \gamma_Q \left|\Gamma^{RX}\right|^2 + Re\left(v^* \Gamma^{RX}\right). \quad (8)$$

Hereinafter, I^{DE} and Q^{DE} will be considered as the normalized output channels for convenience. In order to obtain (7) and (8) three new parameters have been defined:

- DC offset parameter ($\alpha = \alpha_I + j\alpha_Q$)

$$\begin{matrix} \alpha_I = k_3 \left|q_3\right|^2 - k_4 \left|q_4\right|^2 \\ \alpha_Q = k_5 \left|q_5\right|^2 - k_6 \left|q_6\right|^2 \end{matrix} \quad (9)$$

- Rectified wave parameter ($\gamma = \gamma_I + j\gamma_Q$)

$$\begin{matrix} \gamma_I = k_3 - k_4 \\ \gamma_Q = k_5 - k_6 \end{matrix} \quad (10)$$

- Demodulation axes (u and v)

$$\begin{matrix} u = 2\left(k_4 q_4 - k_3 q_3\right) \rightarrow u = u_I + ju_Q \\ v = 2\left(k_6 q_6 - k_5 q_5\right) \rightarrow v = v_I + jv_Q \end{matrix} \quad (11)$$

These four complex constants (α, γ, u, and v), whose meaning will be clarified later on, characterize the demodulator performance. Equations (7) and (8) can be then written in complex form as

$$\Gamma^{DE} = \alpha + \gamma \left|\Gamma^{RX}\right|^2 + \left\{ Re\left(u^* \Gamma^{RX}\right) + jRe\left(v^* \Gamma^{RX}\right) \right\}, \quad (12)$$

or, alternatively, in matrix form as

$$\begin{bmatrix} I^{DE} \\ Q^{DE} \end{bmatrix} = \begin{bmatrix} \alpha_I \\ \alpha_Q \end{bmatrix} + \begin{bmatrix} \gamma_I \\ \gamma_Q \end{bmatrix} \left|\Gamma^{RX}\right|^2 + \begin{bmatrix} u_I & u_Q \\ v_I & v_Q \end{bmatrix} \begin{bmatrix} I^{RX} \\ Q^{RX} \end{bmatrix}. \quad (13)$$

This equation describes the transformation between the received and demodulated symbol planes introduced by any six-port demodulator with analog I/Q generation under homodyne principle and square-law detector regime. From now on, we will designate the three terms appearing at right side of previous (12) and (13) as: DC offset term, rectified wave distortion term, and linear term, respectively.

2.3. Ideal Six-port Demodulator

In an ideal sixport demodulator all the power detectors have the same sensitivity $(R = R_i)$ and a possible set of junction parameters [4] is $S_{41} = S_{51} = S_{62} = \frac{1}{2}$, $S_{42} = -\frac{1}{2}$, $S_{31} = S_{32} = S_{52} = S_{61} = \frac{j}{2}$. Thus, six-port sensitivities are $k_i = \frac{1}{4}$ and its centres fulfill the relations $q_3 = -1$, $q_4 = 1$, $q_5 = -j$ and $q_3 = j$. In this situation $\alpha = 0$, $\gamma = 0$ and $u = -jv = 1$, so (12) becomes

$$\Gamma^{\mathrm{DE}} = \Gamma^{\mathrm{ID}} = u^*\Gamma^{\mathrm{RX}}, \tag{14}$$

which, as seen in Section 2.1 constitutes an ideal demodulator (with constant $U = u^* = 1$ in this specific example). It is clear that, perfect hardware balance has cancelled the DC offset and rectified wave distortion terms, therefore only the desired linear term remains. Furthermore, ideal balance has also caused the demodulated axes to take the ideal quadrature condition $(u = -jv)$. Obviously, hardware impairments will clearly degrade this behavior. In general, any balance imperfection will cause α and γ to be non-zero, and will break the quadrature condition. In the next section we will give a geometrical interpretation of (13) to clarify the effect of each individual term on symbol constellation distortion.

3. SYMBOL CONSTELLATION DISTORTION DUE TO SIX-PORT HARDWARE IMPAIRMENTS

Equations (12) or (13) are the mathematical representation of the transformation that the six-port homodyne receiver establishes between the received Γ^{RX} and demodulated Γ^{DE} symbol planes. From these equations it is clear that the DC offset term does not depend on the received symbol amplitude $|\Gamma^{\mathrm{RX}}|$. The rectified wave term depends on $|\Gamma^{\mathrm{RX}}|^2$, and the desired linear term scales with $|\Gamma^{\mathrm{RX}}|$, where

$$\left|\Gamma^{\mathrm{RX}}\right| = \sqrt{\frac{P_{\mathrm{RX}}}{P_{\mathrm{LO}}}}. \tag{15}$$

The relative influence of the received symbol amplitude can be controlled by means of the amount of signal to LO power in the

demodulator: DC offset (due to $\alpha \neq 0$) will dominate for low $P_{\mathrm{RX}}/P_{\mathrm{LO}}$ ratio, while rectified wave distortion (due to $\gamma \neq 0$) will dominate for high $P_{\mathrm{RX}}/P_{\mathrm{LO}}$ ratio. As a consequence, proper operation of a real six-port will only be possible in some range of $P_{\mathrm{RX}}/P_{\mathrm{LO}}$ ratios and this will intrinsically limit the receiver's dynamic range. Please notice that this effect happens even under ideal square-law detection regime and it is only due to linear imbalances in the sixport junction and detector sensitivities, so it must not be confused with dynamic range limitations coming from higher order nonlinearities of power detectors as analyzed in [13]. This limitation will be of practical importance in optical communication receivers [6], where diode photodetector are intrinsically square law devices and thus dynamic range limitations are expected to appear due to six-port junction impairments.

Once the relative weights of terms appearing in (12) and (13) have been discussed, we will focus on geometrical interpretation of receiver impairments.

3.1. Constellation Distortion due to Linear Impairments

From (13) it is obvious that DC offset and linear terms have a simple interpretation. Effectively, setting $\gamma = 0$, (13) becomes

$$\left[\begin{array}{c} I^{\mathrm{DE}} \\ Q^{\mathrm{DE}} \end{array} \right] = \left[\begin{array}{c} \alpha_I \\ \alpha_Q \end{array} \right] + \left[\begin{array}{cc} u_I & u_Q \\ v_I & v_Q \end{array} \right] \left[\begin{array}{c} I^{\mathrm{RX}} \\ Q^{\mathrm{RX}} \end{array} \right]. \qquad (16)$$

Figure 3 shows the effects of this transformation consisting of a translation α of the origin of coordinates followed by a rotation and imbalance of reference axes.
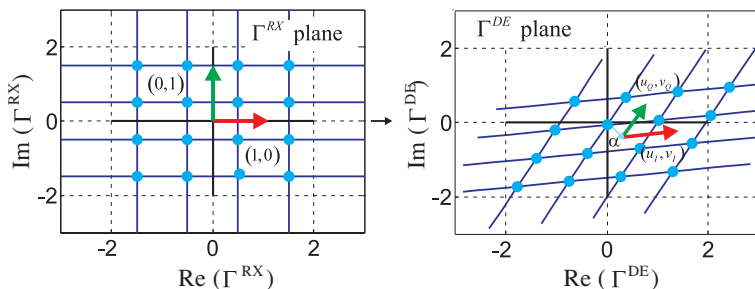

Figure 3. Constellation distortion due to linear impairments in the six-port receiver.

3.2. Constellation Distortion due to Non-linear Impairments

The geometrical interpretation of complete Equations (12) and (13) is more complicated due to the existence of the non-linear rectified wave distortion term (i.e., $\gamma \neq 0$). However, some understanding can be gained by generalizing the well known sixport circle Equations [12] to this particular situation. Effectively, looking at (7) it can be seen that for a fixed value $I^{DE} = I^0$, this equation corresponds to a circle equation in the complex plane whose center (C_I) and radius (R_I) can be easily calculated as

$$C_I = \frac{u}{2\gamma_I}$$
$$R_I = |C_I|^2 - \frac{\alpha_I - I^0}{\gamma_I} = \frac{\sqrt{|u|^2 - 4\gamma_I^*(\alpha_I - I^0)}}{2|\gamma_I|} \quad . \tag{17}$$

The same reasoning can be performed with (8) obtaining similar results. Fig. 4 shows the geometrical interpretation of this situation. The rectangular grid in the demodulated plane Γ^{DE} is the result of the sixport demolulation of circles in the received plane Γ^{RX}. Circle centers always lay on the demodulation axis u and v. When the rectified wave parameter γ approaches zero, the circle centers tend to infinity and the circles become straight lines perpendicular to demodulation axis. This figure gives a beautiful geometric interpretation of sixport with analog I/Q generation similar to the classical one developed for the original sixport [12]. From this interpretation, it is also clear that when $\gamma = 0$ the demodulator establishes a linear transformation between the received and demodulated planes as seen in previous section.
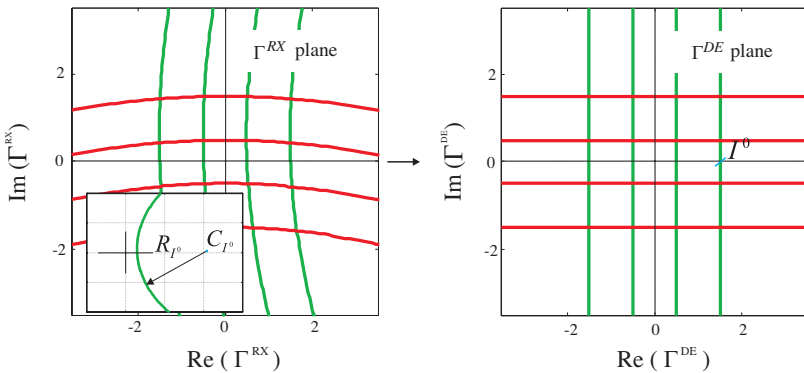

Figure 4. Transformation from circles in the received plane Γ^{RX} to a rectangular grid in the demodulated plane Γ^{DE} due to the rectified wave parameter γ.

4. ERROR VECTOR MAGNITUDE DUE TO SIX-PORT HARDWARE IMPAIRMENTS

In this section we will quantify the effects of constellation distortion on demodulator performance by developing a closed expression to calculate the Error Vector Magnitude [14] (EVM) from sixport parameters α, γ, u and v in (9)–(11).

4.1. EVM Definition

EVM is a well known figure of merit of digital I/Q demodulators [14]. Its meaning can be geometrically understood with the help of Fig. 5(a). In this figure Γ_i^{DE} is the symbol received by the imperfect demodulator under analysis. Γ_i^{ID} the symbol that would be received by an ideal demodulator. The EVM for a symbol i can then be calculated as

$$\mathrm{EVM}_i = \frac{|e_i|}{\left|\Gamma_i^{\mathrm{ID}}\right|} = \frac{\left|\Gamma_i^{\mathrm{DE}} - \Gamma_i^{\mathrm{ID}}\right|}{\left|\Gamma_i^{\mathrm{ID}}\right|}. \tag{18}$$

Finally, the EVM of the receiver for a given constellation is calculated as the root mean square EVM of the set of symbols in the constellation.

4.2. Evaluation of EVM from Hardware Impairments

The main problem in applying (18) for a certain nonideal hardware is the difficulty to identify which is the symbol position for the ideal
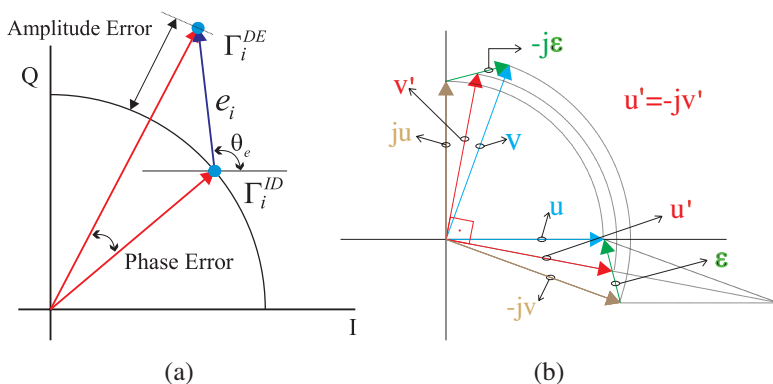

Figure 5. (a) Symbol 'i' error vector magnitude graphical representation. (b) Relation between the non-orthogonal demodulation axes u, v and the to new orthogonal ones u' and v'.

demodulator: as argued in Section 2.1, there is an arbitrary constant, $(U$, see (4)), to be set whose amplitude and phase is related with receiver Automatic Gain Control and Carrier Recovery Subsystem, respectively).

Let's start with the complete receiver equation including all possible impairments ($\alpha \neq 0$, $\gamma \neq 0$, $u \neq -jv$) which we repeat here for convenience

$$\Gamma^{\mathrm{DE}} = \alpha + \gamma \left|\Gamma^{\mathrm{RX}}\right|^2 + \left\{ Re\left(u^* \Gamma^{\mathrm{RX}}\right) + jRe\left(v^* \Gamma^{\mathrm{RX}}\right) \right\}. \qquad (19)$$

The term in brackets of this equation can be interpreted as being the projections of Γ^{RX} on the u and v axes respectively. As in a real situation u and v will not fulfill the ideal orthogonality relation we can define two ideal demodulation axes u' and v' fulfilling the ideal condition $v' = ju'$ and being as close as possible to original ones. This can be achieved by defining

$$\begin{aligned} u' &= \frac{u-jv}{2} \\ v' &= ju' = \frac{v+ju}{2} \end{aligned}. \qquad (20)$$

The situation can be understood with the help of Fig. 5(b), where the relation between the different vectors can be graphically interpreted. In this figure we have also depicted the new variable ε defined as

$$\varepsilon = u + jv, \qquad (21)$$

which is a measure of demodulation axis imbalance.

From (20) and (21) we can write

$$\begin{aligned} u &= u' + \frac{\varepsilon}{2} \\ v &= ju' - j\frac{\varepsilon}{2} \end{aligned}, \qquad (22)$$

and substituting this into (19) and after some algebra we get

$$\Gamma^{\mathrm{DE}} = \alpha + \gamma \left|\Gamma^{\mathrm{RX}}\right|^2 + \left(u'\right)^* \Gamma^{\mathrm{RX}} + \frac{\varepsilon}{2} \left(\Gamma^{\mathrm{RX}}\right)^*. \qquad (23)$$

In this equation the term $\left(u'\right)^* \Gamma^{\mathrm{RX}}$ is easily recognized to be the ideal demodulator symbol position (see (14)), i.e.,

$$\Gamma^{\mathrm{ID}} = \left(u'\right)^* \Gamma^{\mathrm{RX}}, \qquad (24)$$

so the absolute Error Vector can be easily calculated for any symbol i as

$$e_i = \Gamma^{\mathrm{DE}}_i - \Gamma^{\mathrm{ID}}_i = \alpha + \gamma \left|\Gamma^{\mathrm{RX}}_i\right|^2 + \frac{\varepsilon}{2} \left(\Gamma^{\mathrm{RX}}_i\right)^* \qquad (25)$$

and the EVM can be calculated for symbol i as

$$\mathrm{EVM}_i = \left| \frac{\alpha}{|u'|} \left|\Gamma^{\mathrm{RX}}_i\right|^{-1} + \frac{\gamma}{|u'|} \left|\Gamma^{\mathrm{RX}}_i\right| + \frac{\varepsilon}{2|u'|} \frac{\left(\Gamma^{\mathrm{RX}}_i\right)^*}{\left|\Gamma^{\mathrm{RX}}_i\right|} \right|. \qquad (26)$$

This equation is one of the main contributions of this paper as it allows to easily calculate the receiver performance degradation as the vectorial sum of three different contributions. Hence, the following complex numbers can be defined:

- DC rejection

$$R_{\mathrm{DC}} = \frac{\alpha}{|u'|} \qquad (27)$$

- Rectified Wave Rejection

$$R_{\mathrm{RW}} = \frac{\gamma}{|u'|} \qquad (28)$$

- Axis Imbalance

$$I_{\mathrm{A}} = \frac{\varepsilon}{2\,|u'|} = \frac{u + jv}{2\,|u'|} \qquad (29)$$

These three complex numbers completely describe the performance degradation of the demodulator due to hardware impairments and their amplitudes are good figures of merit of demodulator's performance. Notice that in (26) the three terms add vectorially to give the total symbol EVM. Their influence depends on the received symbol amplitude $\left|\Gamma_i^{\mathrm{RX}}\right|$ that in turn depends on the square root of the symbol to LO power ratio as seen in (15).

The worst case scenario occurs with all three terms adding in phase, which allows us to put an upper bound for symbol EVM_i as

$$\mathrm{EVM}_{\mathrm{MAX,i}} = \frac{|R_{\mathrm{DC}}|}{\left|\Gamma_i^{\mathrm{RX}}\right|^{\frac{1}{2}}} + |R_{\mathrm{RW}}| \left|\Gamma_i^{\mathrm{RX}}\right|^{\frac{1}{2}} + |I_{\mathrm{A}}|. \qquad (30)$$

Figure 6(a) shows this symbol EVM upper bound as a funcion of symbol to LO power. It can be clearly observed that DC rejection dominates for low power symbols, rectified wave rejection dominates for high power symbols, and axis imbalance has a constant influence. Furthermore, an optimum point exists when

$$\left|\Gamma_i^{\mathrm{RX}}\right|^2 = \frac{P_{\mathrm{RX,i}}}{P_{\mathrm{LO}}} = \left|\frac{\alpha}{\gamma}\right|, \qquad (31)$$

which minimizes hardware impairment degradation.

However, it is well known that in these sixport receivers improved performance is obtained for low $P_{\mathrm{RX}}/P_{\mathrm{LO}}$ ratios [10, 11], so they are tipically operated at $P_{\mathrm{RX}}/P_{\mathrm{LO}}$ around $-30\,\mathrm{dB}$. This behavior is contradictory with (31) and can only be explained if we take into account that in these cases DC signal is removed using calibration techniques, so the effect of R_{DC} is corrected by calibration. In fact, if $R_{\mathrm{DC}} = 0$, (30) also predicts a better performance for lower $P_{\mathrm{RX}}/P_{\mathrm{LO}}$
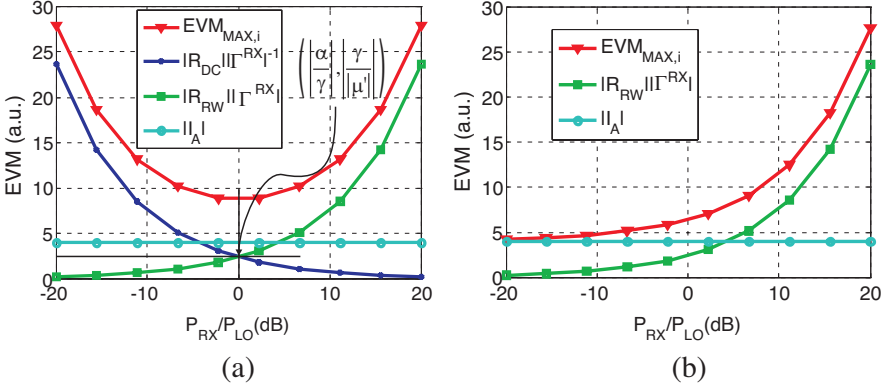
Figure 6. Symbol EVM upper bound as a function of symbol to LO power and the effects of the three different contributions of (30). (a) Including R_{DC}. (b) Removing R_{DC}.

ratios, as shown in Fig. 6(b). Now, the effect of the rectified wave rejection can be reduced increasing the LO power, so EVM tends to I_A, which stablishes the minimum EVM of a specific receiver. The minimum symbol to LO power ratio will be fixed by power detectors since: i) a minimum RF power signal is needed to be detectable, and ii) higher order nonlinearities limit the maximum LO power. In the following sections it will be assumed that calibration removes DC signal term (i.e., $R_{DC} = 0$).

5. ERROR PROBABILITY DUE TO HARDWARE IMPAIRMENTS

The errors in symbol reception due to hardware impairments increase the error probability. Hence, both of them must be related to set the receiver hardware specifications from error probability and signal-to-noise ratio (SNR) specifications.

For determining the error probability a modulation technique must be chosen. In this case, a QPSK modulation is used. Besides, the received signal is modeled including additive white Gaussian noise (AWGN). In an ideal case, the received constellation in presence of noise is as depicted in Fig. 7(a), and the symbol error probability is [15]:

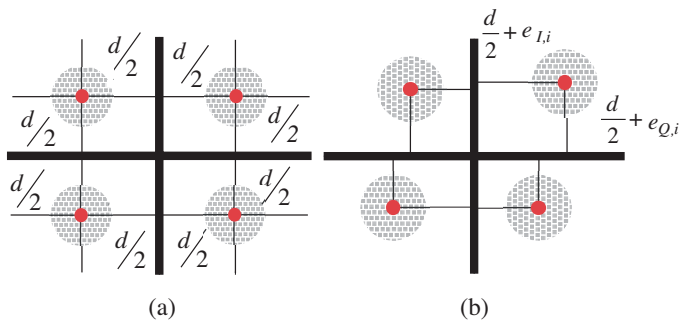$$P_{e_i} = 2Q\left(\frac{d}{2\sigma}\right) = 2Q\left(\sqrt{2\,\mathrm{SNR}}\right) \tag{32}$$

Figure 7. Received QPSK constellation. (a) In an ideal receiver. (b) In a real receiver.

Due to hardware impairments, signal and noise will suffer a distortion as predicted by (12). However, for small hardware impairments, typically required to assure a low BER, it can be assumed that constellation distortion mostly affects the symbol positions but not the noise gaussian distribution. This basic idea is illustrated in Fig. 7(b) where it is shown that symbol position is modified by hardware impairments but the noise contributions are still considered as two dimensional uncorrelated Gaussians. This assumption will be shown in Section 6 to be correct for small hardware impairments and low symbol to LO power ratios. The translation suffered by every symbol can be calculated u sing (25). Thus, the error probability of a received symbol is

$$P_{e_i} = Q\left(\sqrt{2\,\mathrm{SNR}} + \frac{Re\,(e_i)}{\sigma}\right) + Q\left(\sqrt{2\,\mathrm{SNR}} + \frac{Im\,(e_i)}{\sigma}\right), \quad (33)$$

and substituting σ using the SNR formula in a QPSK modulation [15] the symbol error probability can be rewritten as:

$$P_{e_i} = Q\left(\sqrt{2\mathrm{SNR}} + \frac{Re(e_i)\sqrt{4\mathrm{SNR}}}{|\Gamma_i^{\mathrm{RX}}|}\right) + Q\left(\sqrt{2\mathrm{SNR}} + \frac{Im(e_i)\sqrt{4\mathrm{SNR}}}{|\Gamma_i^{\mathrm{RX}}|}\right) (34)$$

Equation (34) is very significant as it allows to determine the error probability of each symbol relating it to the Error Vector shown in (25). In order to get an easier formulation, (34) is approximated by a second order Taylor series, so the error probability can be calculated from the SNR and the EVM (see Appendix A). Furthermore, since all QPSK symbols have the same energy, and probability, the EVM_i of all symbol will be similar. In this case, assuming the worst case scenario and a
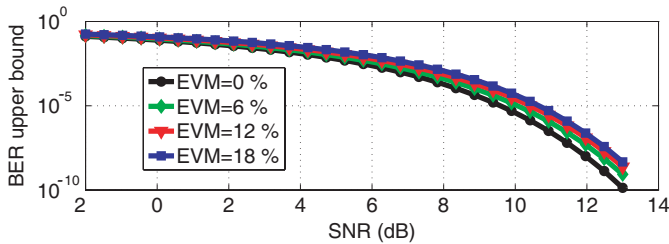
Figure 8. BER upper bound for different EVM.

Gray codification, an upper bound for the Bit Error Ratio (BER) is determined by

$$\mathrm{BER} = Q\left(\sqrt{2\mathrm{SNR}}\right) + \frac{1}{\sqrt{\pi}} \exp\left(-\mathrm{SNR}\right) \mathrm{EVM}\sqrt{\mathrm{SNR}} \left[1 + \mathrm{SNR\,EVM}\right]$$

(35)

Equation (35) is very interesting as it lets designers know the maximum EVM that achieves a certain BER for a QPSK receiver. Once the maximum EVM is known, it can be used to get the initial specifications of all the receiver elements. In Fig. 8, BER as a function of SNR for different values of EVM is depicted using (35). It can be clearly seen that a 12 % EVM entails a 1 dB SNR penalty for a typical BER of 10^{-3}.

6. ANALYSIS OF A SPECIFIC SIX-PORT ARCHITECTURE

In this section a specific six-port receiver architecture is studied using the proposed formula for EVM. Subsequently, in Section 7, formulas for EVM, BER and their relationship will be validated. The chosen architecture is based on a well known model [1] comprised of three hybrids and a power divider, as shown in Fig. 9. The objective is to understand its behavior and analyse its degradation. The hardware impairments considered in this analysis are the imbalances of the power divider and quadrature hybrids in the sixport junction, as defined in Fig. 9. In all cases, the three hybrids have been supposed to be identical, i.e., we have neglected any possible imbalance due to fabrication tolerances. Applying the equations defined in Fig. 9 in (9)–(11) and (28)–(29), after some manipulation, the figures of merit for this architecture can be calculated as

$$R_{\mathrm{RW}} = \frac{-k_\gamma \left[\left(1 - |I_H|^2\right) + j\,|I_H|\left(|I_H|^2 - 1\right)\right]}{|u'|},$$
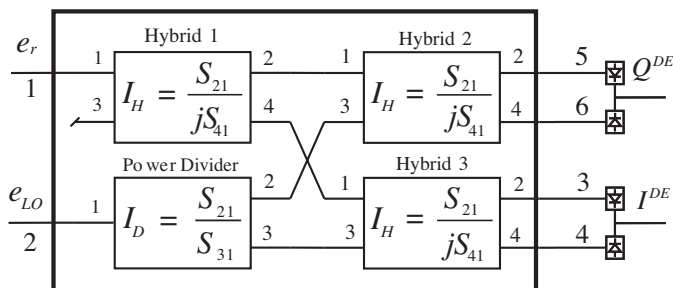
(36)

Figure 9. Analysed six-port receiver architecture comprised of three hybrids and a power divider. The defined parameters I_H and I_D are the hybrid and power divider imbalances respectively.

$$I_A = \frac{1 - |I_D| \, |I_H| \exp\left[j \left(\measuredangle I_D - \measuredangle I_H\right)\right]}{|1 + |I_D| \, |I_H| \exp\left[j \left(\measuredangle I_D - \measuredangle I_H\right)\right]|}. \tag{37}$$

where I_D, I_H are the power divider and hybrid imbalances defined in Fig. 9, and k_γ depends on the sixport elements' S parameters. It must be noticed that the DC signal term has been corrected by calibration, so R_{DC} has been set to 0.

In order to understand the effect of these figures of merit (36)–(37) several results will be presented. Initially, sixport's EVM is calculated as a function of the power divider imbalances, assuming that all the hybrids are ideal (i.e., $I_H = 0$). In this case, from (36)–(37) it can be observed that $R_{\mathrm{RW}} = 0$ and EVM only depends on the axis imbalance (I_A) following the relationship,

$$\mathrm{EVM} = I_A = \frac{1 - |I_D| \exp\left(j\measuredangle I_D\right)}{|1 + |I_D| \exp\left(j\measuredangle I_D\right)|}. \tag{38}$$

The calculated EVM contour map is depicted in Fig. 10. It shows that any phase or amplitude imbalance in the power divider (I_D) will degrade EVM when hybrids are ideal, and that the power divider phase imbalance $(\measuredangle I_D)$ is more important than the amplitude imbalance $(|I_D|)$ in this case.

Now a more realistic situation will be analyzed and the sixport receiver EVM will be calculated as a function of the hybrids imbalance, fixing a power divider amplitude and phase imbalance of $1\,\mathrm{dB}$ and $5°$, respectively. In this case, $R_{\mathrm{RW}} \neq 0$ and some very interesting features of this particular situation can be observed. Analysing (37) it is clear that when $\measuredangle I_D = \measuredangle I_H$, their effects are mutually cancelled and EVM is improved, as shown in Fig. 11. Even though $R_{\mathrm{RW}} \neq 0$, its effect can be clearly minimized, as was demonstrated in Section 4. In this situation the symbol to LO power ratio becomes crucial as
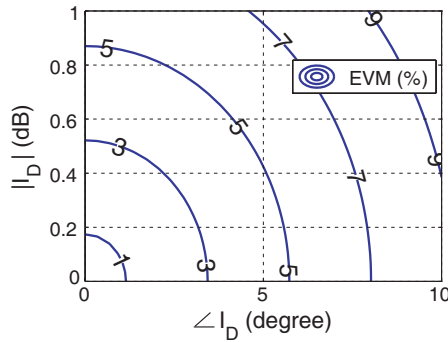
Figure 10. Calculated EVM using (26) and (38) as a function of the power divider imbalance (I_D) amplitude and phase, when quadrature hybrids are ideal.
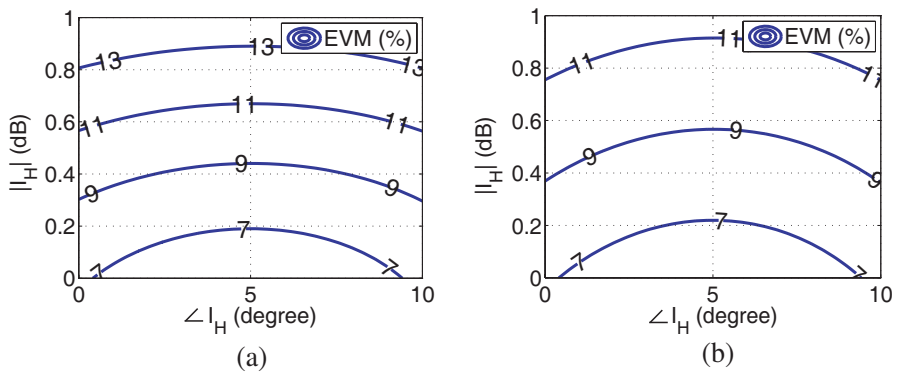

Figure 11. Calculated EVM (26) of the analysed six-port architecture as a function of hybrid coupler imbalance for a given power divider imbalance (amplitude and phase imbalances of $1\,\mathrm{dB}$ and $5°$ respectively). (a) $P_{\mathrm{RX}}/P_{\mathrm{LO}} = 0\,\mathrm{dB}$. (b) $P_{\mathrm{RX}}/P_{\mathrm{LO}} = -30\,\mathrm{dB}$.

shown in Fig. 11. When the sixport receiver works with a symbol to LO power ratio close to $0\,\mathrm{dB}$, the error introduced by R_{RW} is still comparable to I_A and EVM (shown in Fig. 11(a)) is degraded. However, if the receiver works with a lower symbol to LO power ratio ($P_{\mathrm{RX}}/P_{\mathrm{LO}} = -30\,\mathrm{dB}$ for instance), its effect is minimized and EVM is clearly improved, as depicted in Fig. 11(b). Even though it seems that the effect of R_{RW} can be cancelled in any situation only decreasing $P_{\mathrm{RX}}/P_{\mathrm{LO}}$, there is a minimum power ratio fixed by power detectors, as was explained in Section 4. Working below this minimum power

ratio, power detectors (not considered in our analysis) will degrade EVM. Hence, the optimum operation point will depend on the specific sixport receiver realization.

The analysis performed in this section has shown the importance of EVM Equation (26) and its three figures of merit (R_{DC}, R_{RW} and I_A). They can be used to obtain simple formulas for any sixport architecture as (36)–(37) that allow to get a deeper insight into its behavior and even determine the component requirements.

7. VALIDATION OF THE PROPOSED FORMULAS

Once the utility of EVM Equation (26) to analyse an specific six-port architecture and understand its degradation has been stated, in this section we will verify the accuracy of proposed formulas for EVM (26) and BER (34). To do that, a simple microstrip sixport architecture with a 6.85 GHz central frequency has been designed using Agilent ADS circuital simulator (see Fig. 12(a)). It is based on the sixport architecture studied in Section 6 and is comprised of a Wilkinson power divider (see Fig. 12(b)) and three coupled-lines hybrid couplers. In its design, a 4350B Roger substrate with a thickness of 0.305 mm and $\epsilon_r = 3.66$ has been chosen.

The proposed formulas have been used to evaluate the performance of this six-port receiver, showing a good accuracy in its operation bandwidth. The designed architecture is a narrowband circuit whose performance is clearly degraded below 4.7 GHz and above 9 GHz. In this section, the results obtained in its evaluation at 9 GHz are presented. At this frequency point the effect of: i) DC offset
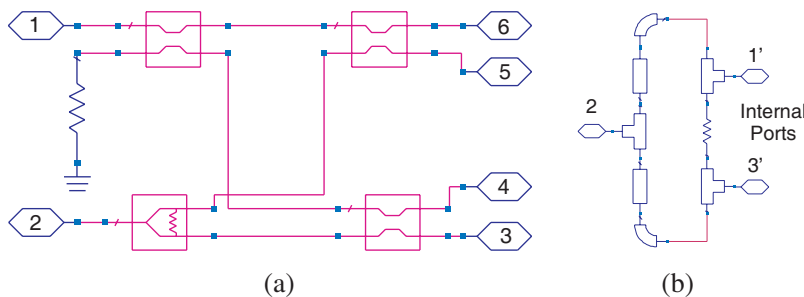

(a)   (b)

Figure 12. Microstrip six-port architecture used in the validation of the proposed formulas. It is comprised of a Wilkinson power divider and three coupled-lines hybrid couplers. (a) General scheme. (b) Wilkinson power divider scheme.

parameter (α), ii) rectified wave parameter (γ), and iii) demodulation axes imbalances (u and v) are patent, but the sixport performance can be still acceptable.

This section is divided in three parts. In the first part, the estimated EVM (26) is compared with the simulated one in absence of noise. In the second part, the relationship between EVM and BER is demonstrated. Finally, in the third part, the estimated BER (34) is compared with the simulated one.

7.1. Validation of the EVM Formula

In order to verify the proposed formula for EVM (26), the reception of QPSK symbols in absence of noise has been simulated, using both Automatic Gain Control (AGC) and carrier recovery by means of the fourth-power method [16, pp. 511]. At 9 Ghz the coupled lines of the sixport architecture are strongly unbalanced ($|I_H| = 1.2\,\text{dB}$, $\angle I_H = 5.3°$). However, the Wilkinson power divider does not present any imbalance ($|I_D| = 0\,\text{dB}$, $\angle I_D = 0°$), as expected in a symmetrical circuit. Assuming that DC signal has previously been cancelled by calibration ($R_{\text{DC}} = 0$), only the rectified wave signal (R_{RW}) and axis imbalances (I_A) degrade EVM. The results of the simulated and theoretical EVM (26) with its different terms as a function of the symbol to LO power are depicted in Fig. 13. It shows that decreasing the power to LO signal ratio EVM can be partially improved. Besides, it demonstrates that (26) can model the EVM of a real sixport architecture, as simulated and theoretical results are almost coincident.
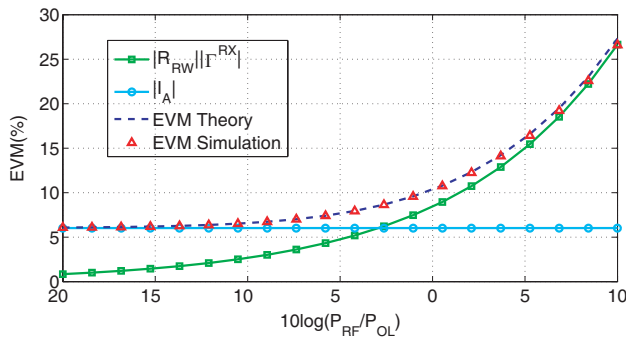

Figure 13. Simulated and calculated EVM (26) as a function of symbol to LO power including the calculated effects of its different contributions in absence of noise.
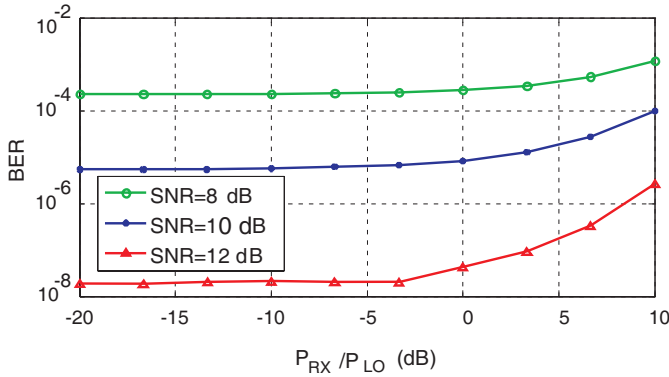
Figure 14. Simulated BER as a function symbol to LO power ratio for different SNR using the designed sixport architecture at 9 GHz.

7.2. Relationship between EVM and BER

Previous considerations show that when DC signal is cancelled EVM is minimized when P_{RX}/P_{LO} is decreased. Now, it will be proven that in this case, the reduction of P_{RX}/P_{LO} also provides an optimum BER performance. To show this, the reception of a QPSK signal with AWGN is simulated using the designed sixport architecture at 9 GHz, as in the previous subsection, so that the results can be directly compared. Fig. 14 shows that best performance of the receiver is obtained when P_{RX}/P_{LO} is decreased (BER is minimized for the same SNR). However, there is only a slight improvement when P_{RX}/P_{LO} is reduced from -10 dB to -20 dB. This result agrees with those in Fig. 13 in which it can be clearly seen that for P_{RX}/P_{LO} ratios below -10 dBm the effect of R_{RW} is much lower than the effect of the axis imbalance I_A and thus there is no improvement in EVM for decreasing values of the P_{RX}/P_{LO} ratio. Although not presented for the sake of brevity, this type of plot has been repeated for several frequency points and the same behavior has been observed.

7.3. Validation of the BER Formula

The reception of a QPSK signal with AWGN is simulated again, using the designed sixport architecture at 9 GHz for different symbol to LO power ratios, in two situations: i) when DC signal remains, and ii) when DC signal is cancelled by calibration. In the first case, BER is completely degraded when the symbol to LO power ratio is reduced, as depicted in Fig. 15(a). It happens because R_{DC} has not been removed,
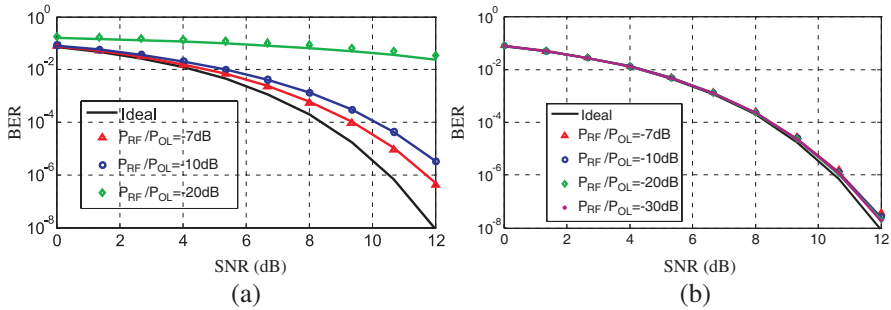
Figure 15. Simulated and calculated BER (34) as a funcion of SNR for different symbol to LO power. Coloured continuous line and marks are the simulated and calculated results, respectively for a specific symbol to LO power. (a) When DC signal is not removed, $R_{DC} \neq 0$. (b) When DC signal is removed, $R_{DC} = 0$.

so the DC term becomes the principal impairment, translating the symbols of the QPSK modulation from their decision region. However, if the DC signal is removed by calibration, best BER results are obtained when P_{RX}/P_{LO} is reduced, as shown in Fig. 15(b). Therefore, it is important to emphasize that it is crucial the implementation of a good technique to remove the DC signal when lower signal to LO power ratios are going to be used in these sort of receivers. Finally, Fig. 15 clearly shows that theoretically calculated results (marks) are in very good agreement with simulated results (lines), so (34) can be used for a good engineering estimation of system BER in practical sixport communications receivers, where LO power is much greater than RX power.

8. CONCLUSION

In this paper a detailed study of the analog I/Q generation six-port receiver has been carried out. In doing so, three complex parameters have been defined (R_{DC}, R_{RW} and I_A), which completely describe constellation distortion due to hardware impairments of the six-port junction, thus allowing to directly calculate the receiver's EVM and evaluate its performance degradation. This is an important result of this work as it establishes that six-port performance can be completely described only with three complex number instead of using the 8 scattering parameters (8 complex numbers) plus the four detector's sensitivities (4 real parameters) that originally define the receiver hardware.

Simplified approximate formulas have been also obtained which allow to easily calculate BER degradation due to hardware impairments, from the previously defined parameters. These are interesting closed expressions which easily allow to set sixport hardware specifications to fulfill certain BER requirements. Altough the formulas have been derived for QPSK modulation, they could be easily extended to other modulation techniques.

A six-port receiver architecture comprised of three hybrids and a power divider have been analysed using the three complex parameters (R_{DC}, R_{RW} and I_A) to get a deeper understanding of its behaviour. Finally, the assessment of the proposed expressions has been carried out by comparing the theoretically predicted EVM and BER, under AWGN, with the simulated ones for a specific microstrip sixport architecture, as a function of the P_{RX}/P_{LO} ratio.

ACKNOWLEDGMENT

APPENDIX A. ERROR PROBABILITY APPROXIMATION FOR QPSK MODULATION

The error probability of a received symbol as a consequence of hardware impairments is stated in (33) or (34). The Q function can be rewritten using a Taylor series with an infinite sum of terms, but in this case a second degree polynomial has been used

$$Q(x) \approx Q(x_0) + Q'(x_0)(x - x_0) + \frac{Q''(x_0)}{2}(x - x_0)^2. \quad \text{(A1)}$$

This approximation is valid for good performance receivers. Then, using (A1) in (33) and substituting

$$\frac{|e_i|^2}{\sigma^2} = \frac{|e_i|^2}{\left|\Gamma_i^{ID}\right|^2} \frac{\left|\Gamma_i^{ID}\right|^2}{\sigma^2} = 4\,\text{SNR}\,\text{EVM}_i^2, \quad \text{(A2)}$$

$$\frac{Re(e_i) + Im(e_i)}{\sigma} = \sqrt{4\,\text{SNR}\,\text{EVM}_i^2}\left(\cos\theta_{e_i} + \sin\theta_{e_i}\right), \quad \text{(A3)}$$

after some algebra the approximated symbol error probability can be deduced as

$$P_{e_i} = 2Q\left(\sqrt{2\mathrm{SNR}}\right) -$$

$$-\frac{1}{\sqrt{\pi}}\exp\left(-\mathrm{SNR}\right)\mathrm{EVM}_i\sqrt{\mathrm{SNR}}\left[\sqrt{2}\left(\cos\theta_{e_i} + \sin\theta_{e_i}\right) - 2\mathrm{SNR}\,\mathrm{EVM}_i\right], (A4)$$

where θ_{e_i} is the vector error angle of the received symbol (see Fig. 5(a)). As evident from (A4), the symbol error probability depend on the symbol position. Hence, the worst case can be assumed ($\theta_{e_i} = 225°$) to get an upper bound.

REFERENCES

1. Li, R., R. G. Bosisio, and K. Wu, "A six-port digital millimeter wave receiver," *IEEE MTT-S International Microwave Symposium Digest*, 1994.

2. Tatu, S. O., E. Moldovan, K. Wu, and R. G. Bosisio, "A new direct millimeter-wave six-port receiver," *IEEE Transactions on Microwave Theory and Techniques*, Vol. 49, No. 12, 2517–2522, Dec. 2001.

3. Mallat, K., E. Moldovan, and S. O. Tatu, "Comparative demodulation results for six-port and conventional 60 GHz direct conversion receivers," *Progress In Electromagnetics Research*, Vol. 84, 437–449, 2008.

4. Pérez-Dueñas, J., J. G. Wangümert-Pérez, and I. Molina-Fernández, "Novel modulation scheme and six-port based rake receiver for DS-UWB," *IEEE Transactions on Wireless Communications*, Vol. 8, No. 7, 3628–3633, Jul. 2009.

5. Seimetz, M. and C.-M. Weinert, "Options, feasibility, and availability of 2×4 90° hybrids for coherent optical systems," *Journal of Lightwave Technology*, Vol. 24, No. 3, 1317–1322, Mar. 2006.

6. Kunkel, R., H.-G. Bach, D. Hoffmann, C. M. Weinert, I. Molina-Fernandez, and R. Halir, "First monolithic InP-based 90°-hybrid OEIC comprising balanced detectors for 100GE coherent frontends," *IEEE International Conference on Indium Phosphide & Related Materials*, May 2009.

7. "Implementation Agreement for Integrated Dual Polarization Intradyne Coherent Receivers," *Optical Internetworking Forum,* Apr. 2010. Available: http://www.oiforum.com/public/documents/OIF_DPC_RX-01.0.pdf.

8. Pérez-Lara, P., I. Molina-Fernández, and J. G. Wangümert-Pérez, "Effects of hardware imperfection on six-port direct digital receivers calibrated with three and four signal standards," *IEE Proceedings Microwaves, Antennas and Propagation*, Vol. 153, No. 2, 171–176, Apr. 2006.

9. Henstschel, T., "The six-port as a communications receiver," *IEEE Transactions on Microwave Theory and Techniques*, Vol. 53, No. 3, 1039–1047, Mar. 2005.

10. Winter, S. M., H. J. Ehm, A. Koelpin, and R. Weigel, "Analysis of system parameters of a six-port communications receiver with analog I/Q regeneration," *International Sympodium on Signal, Systems and Electronics*, 375–378. Jul. 2007.

11. Winter, S. M., H. J. Ehm, A. Koelpin, and R. Weigel, "Diode power detector dc operating point in six-port communications receivers," *Proceedings of the 37th European Microwave Conference*, 795–798, Oct. 2007.

12. Engen, G. F., "The six-port reflectometer: An alternative network analyzer," *IEEE Transactions on Microwave Theory and Techniques*, Vol. 25, No. 12, 1075–1079, Dec. 1977.

13. Mailand, M., R. Richter, and H.-J. Jentschel, "Nonlinearity analysis of power detectors in direct conversion receivers utilizing six-port technology," *International Symposium on Signals, Circuits and Systems*, 123–126, Sep. 2005.

14. McKinley, M. D., K. A. Remley, M. Myslinski, J. S. Kenney, D. Schreurs, and B. Nauwelaers, "EVM calculation for broadband modulated signals," *Proceedings of the 64th ARFTG Conference*, 45–52, Dec. 2004.

15. Proakis, J. G., *Digital Communications*, 4th edition, MacGraw-Hill, Aug. 2000.

16. Jeruchim, M. C., P. Balaban, and K. S. Shanmugan, *Simulation of Communication Systems Modelling Methodology, and Techniques*, 2nd edition, Kluwer Academic/Plenum Publishers, 2000.